minerals

MDPI

Article

Mortars in the Archaeological Site of Hierapolis of Phrygia (Denizli, Turkey) from Imperial to Byzantine Age

Matteo Maria Niccolò Franceschini [1,2], Sara Calandra [3], Silvia Vettori [1], Tommaso Ismaelli [1], Giuseppe Scardozzi [4], Maria Piera Caggia [4] and Emma Cantisani [1,*]

[1] Institute of Heritage Science, Via Madonna del Piano, 10-50019 Florence, Italy; matteo.franceschini@ispc.cnr.it (M.M.N.F.); silvia.vettori@cnr.it (S.V.); tommaso.ismaelli@cnr.it (T.I.)
[2] Department of Science of Antiquities, Sapienza University of Rome, Piazzale Aldo Moro, 5-00185 Roma, Italy
[3] Earth Science Department, University of Florence, Via La Pira, 4-50121 Florence, Italy; sara.calandra@unifi.it
[4] Institute of Heritage Science, Via Prov. le Lecce-Monteroni, 73100 Lecce, Italy; giuseppe.scardozzi@cnr.it (G.S.); mariapiera.caggia@cnr.it (M.P.C.)
* Correspondence: emma.cantisani@cnr.it

Abstract: Hierapolis of Phrygia, an archaeological site in southwestern Turkey, has been a UNESCO World Heritage Site since 1988. During archaeological campaigns, 71 mortar samples from public buildings were collected, dating from the Julio-Claudian to the Middle Byzantine period. The samples were analyzed using a multi-analytical approach including polarized optical microscopy (POM), digital image analysis (DIA), X-ray powder diffraction (XRPD) and SEM–EDS to trace the raw materials and understand the evolution of mortar composition and technology over time. During the Roman period, travertine and marble were commonly used in binder production, while marble dominated in the Byzantine period. The aggregates come mainly from sands of the Lycian Nappe and Menderes Massif, with carbonate and silicate rock fragments. Variations in composition, average size and circularity suggest changes in raw material sources in both Roman and Byzantine periods. *Cocciopesto* mortar was used in water-related structures from the Flavian to the Severan period, but, in the Byzantine period, it also appeared in non-hydraulic contexts. Straw became a common organic additive in Byzantine renders, marking a shift from the exclusively inorganic aggregates of Roman renders. This study illustrates the evolving construction technologies and material sources used throughout the city's history.

Keywords: Hierapolis; mortar-based materials; raw material evolution; technologies of production; Roman period; Byzantine period

Citation: Franceschini, M.M.N.; Calandra, S.; Vettori, S.; Ismaelli, T.; Scardozzi, G.; Caggia, M.P.; Cantisani, E. Mortars in the Archaeological Site of Hierapolis of Phrygia (Denizli, Turkey) from Imperial to Byzantine Age. *Minerals* **2024**, *14*, 1143. https://doi.org/10.3390/min14111143

Academic Editor: Domenico Miriello

Received: 19 September 2024
Revised: 28 October 2024
Accepted: 5 November 2024
Published: 11 November 2024

1. Introduction

In recent years, many scholars have been engaged in the study of mortars and plasters used in buildings of cultural interest, following a well-established protocol for the petrographic, mineralogical and geochemical characterization of these materials [1–7]. Numerous papers have emphasized the importance of mineralogical and chemical properties of mortar-based materials to find the provenance of raw materials [8–10], while other studies have focused on the mechanical properties of mortars to assess the state of the conservation of masonry [11]. In some cases, the study of mortar-based materials has made it possible to distinguish different construction phases of buildings based on the evolution of the technology for producing mortar and the choice of raw materials over time [12–18]. With a similar perspective, the present work examines the changes in the selection of raw materials and the production technologies of mortar-based materials belonging to public buildings of Hierapolis, from the Roman to the Middle Byzantine period. The geographical location and the long history of Hierapolis of Phrygia have made this city particularly interesting for archaeometric research (Figure 1). The earthquakes that damaged or destroyed it several times have left traces both in the historical sources and

in the archaeological evidence, and this makes Hierapolis an excellent case study for the identification of different construction phases and archaeometric approach on materials [19]. Thanks to the accurate study of the public buildings of Hierapolis and the stratigraphic excavations carried out by the Italian Archaeological Mission since 1957, a solid grid of archaeological dating has been created on which scientific analyses of mortars and plasters can be based in order to trace the areas of the supply of their raw materials and to assess the evolution of the technologies used in the production of these materials over time. In this work, the petrographic, mineralogical and chemical characterizations of mortar samples were performed with a well-established methodological approach, combined with the digital image analysis of selected samples, to highlight continuity and changes in the use of raw materials and technologies employed for the production of mortar-based materials.

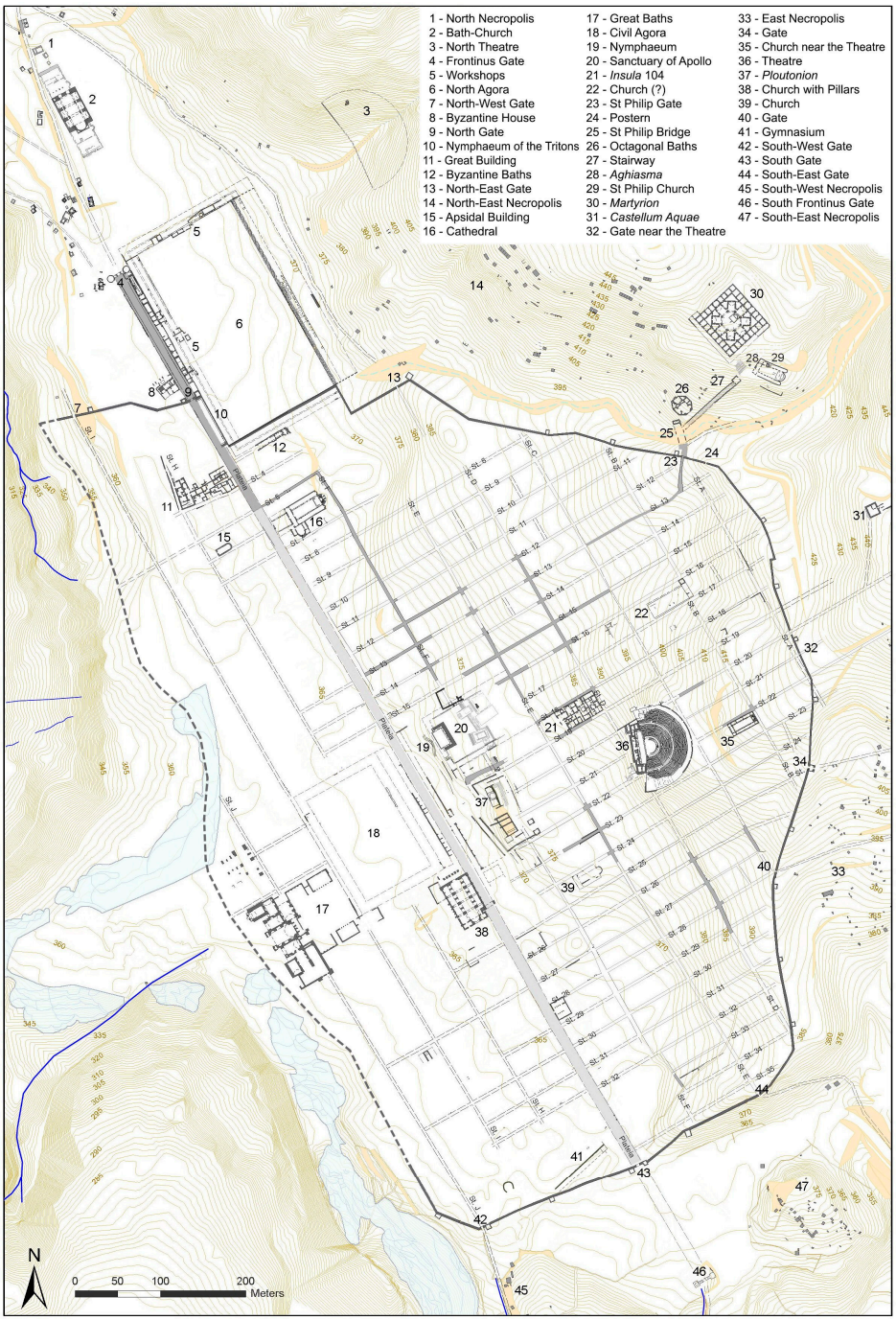

Figure 1. Plan of the ancient city of Hierapolis.

Geological Setting

The archaeological site of Hierapolis (Denizli, Turkey), located in western Anatolia, was founded in the 3rd century BCE and, even if damaged several times by earthquakes [17–19], the city was inhabited and restored until the Mediaeval period. From a geological point of view, this area is characterized by the presence of metamorphic rocks associated with the alpine metamorphic dome of Menderes Massif [20–24]. From the Miocene to the present day, the continuing extensional tectonics has divided the Menderes Massif into three sub-massifs due to the formation of three large grabens: the Küçük Menderes, the Büyük Menderes and the Gediz (Figure 2a). These converge into the Denizli Graben, which lies on the south-eastern edge of the Menderes Massif and borders on the Lycian Nappe. The area is characterized by normal faulting to the southwest by the Babadağ main fault and to the northeast by the Pamukkale fault zone. This fault zone includes the world-famous terrace of Pamukkale [25–28], known for its white travertine waterfalls of calcareous deposits originated from thermal water, which gave the terrace its name ("Pamukkale" means "cotton castle") [16]. The extensional tectonics of the Anatolian region is the main cause of the territory faulting and magmatic intrusions. This condition explains the heating of meteoric waters deeply entering the soil through fractures and faults, which cause the formation of numerous hydrothermal springs, with more or less high temperature [29,30]. The prolonged discharge of hot, $CaCO_3$-rich fluids from faults, fissures and rock fractures have led to massive depositions of bedded and banded travertines, which have been extensively exploited over time [31]. These hydrothermal fluids are also involved in forming carbonate-cemented breccia produced by the cementation of sedimentary or metamorphic rock debris [32,33]. Marbles are abundant in the surroundings of Hierapolis, with ancient quarries located only a few kilometers from the city center. This rock type is linked to the metamorphic Menderes Massif [34,35], as well as the other metamorphic rocks outcropping in the Hierapolis area: quartzites, calc-schists, meta-sandstones, phyllites, schists, amphibolites and gneisses (Figure 2b). Within the Denizli basin, we can observe some allochthonous rock outcrops, belonging to the Lycian Nappe, that is the upper thrust sheet that overlies the metamorphic Menderes Massif in south-western Turkey [36,37]. The Lycian Nappe tectonic unit consists mainly of sedimentary Mesozoic carbonate rocks. The ophiolites, which are of oceanic origin (Late Cretaceous), form the upper thrust sheet of the sedimentary units [38]. Regarding geomorphology, the remains of Hierapolis lie on a travertine platform on the Pamukkale fault zone, which is constantly subjected to the deposition of travertine due to hydrothermal activities. At the macroscopic scale, the Pamukkale terrace overlooks the plain of the Lykos River, the current Çürüksu River and a lake in the plain, dry today, but that had various tributaries, such as streams flowing near Laodicea, the Kadmos (Gökpınar-Karakurt) and the Asopos (Gümüşçay-Goncalı) [39], which still descend from the foothills of Mount Babadağ and cut through a small horst separating the Çürüksu River valley from the Denizli area. The plain is surrounded by Mount Babadağ (in the south), the Uzunpınar plateau and the Küçükçökelez massif (in the north) [40], Mount Honaz (in the southwest) and Mount Sazak (in the west) [39], but there is no topographical obstacle in the northeast [41]. Therefore, the Çürüksu collects the streams and the small seasonal rivers flowing from the surrounding ridges characterized by narrow valleys. This is the case of the Gök Dere, Suini Dere and the Kadı Dere, which flow down near Hierapolis [33,42]. The Çürüksu river, originating from the confluence of Saraçay creek and Alikurt creek [43], ends its journey near Sarayköy, where it flows into the Maeander River, which represents the natural connection between the Aegean Sea and inner south-western Anatolia.

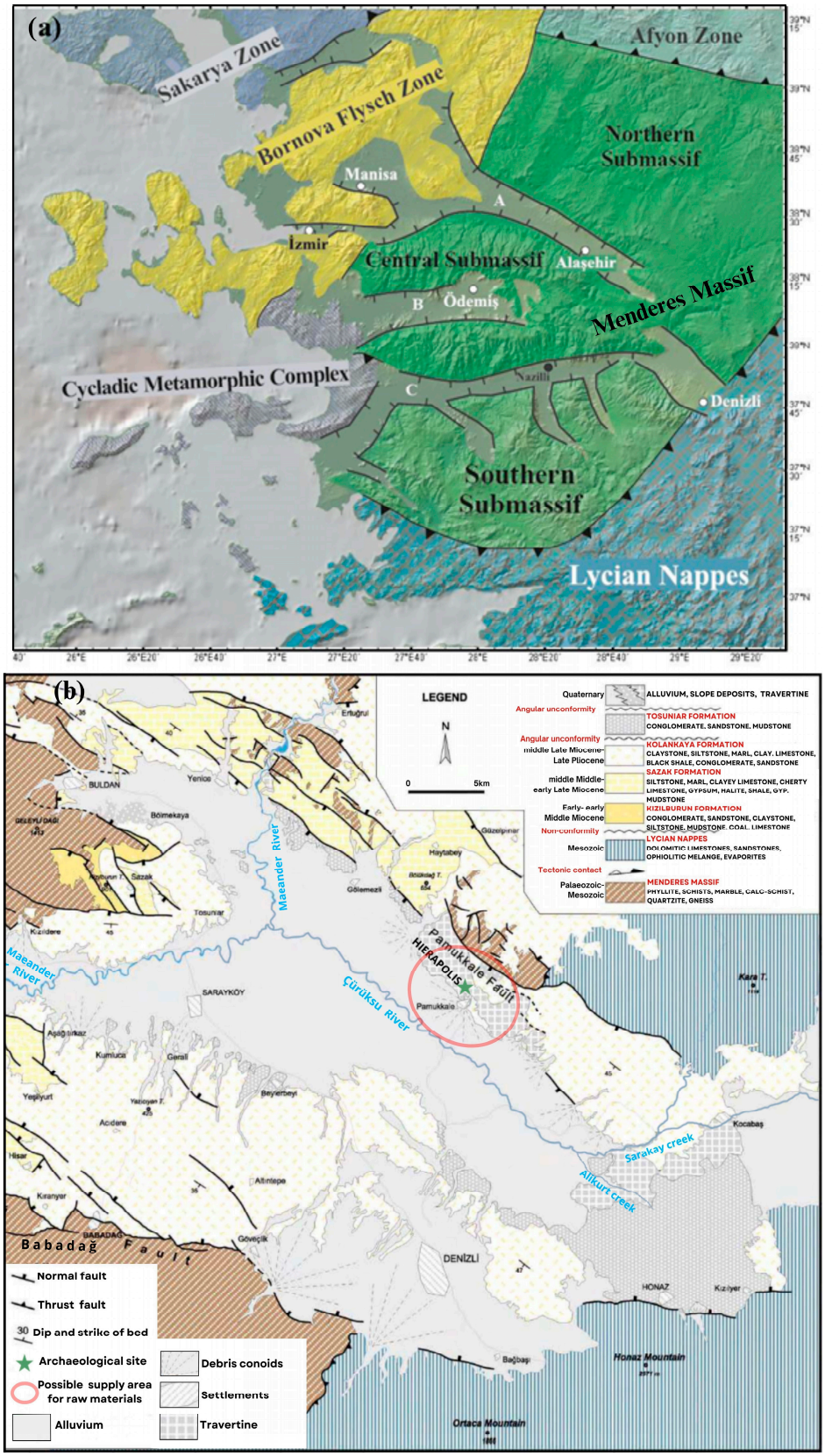

Figure 2. (**a**) Tectonic map of western Anatolia (A: Gediz or Alaşehir Graben, B: Küçük Menderes Graben and C: Büyük Menderes Graben), modified from [44]; (**b**) geological map of the Denizli Basin (modified from [45]).

2. Materials and Methods

This study involves 71 samples of mortar-based materials taken from the following main monuments of Hierapolis: the Apollo Sanctuary, Building C (Julio-Claudian period, about late 1st century BCE—60 CE), the Ploutonion (60 BCE—Early Byzantine period); the Stoa of the Springs (Neronian—54–68 CE, Flavian—68–96 CE and uncertain dating structures), the Great Building—Roman Baths (Flavian period), the Nymphaeum of the Apollo Sanctuary (Late Antonine period, about 160–180 CE); the Theatre (Severan period, 192–235 CE), the Nymphaeum of the Tritons (Severan period, beginning of the 3rd century CE), the Apollo Sanctuary, Building A (Severan—Early Byzantine period) and the Church of St. Philip (4th century CE–11th century CE) (Figures 1 and 3) [22].

Figure 3. Some of the main monuments of Hierapolis: (**a**) The Apollo Sanctuary, Building A; (**b**) the Stoa of the Springs; (**c**) Nymphaeum of the Tritons; (**d**) the Theatre; (**e**) the Ploutonion; and (**f**) Church of St. Philip.

Specifically, based on the accurate study of wall stratigraphy, the study of building technique, building materials and decorative-painting apparatus, 31 samples belong to buildings dating from the Julio-Claudian period to the Early Byzantine period, and 40 samples from the Church of St. Philip, covering from the Early Byzantine to the Middle Byzantine period, were taken. In this context, it was possible to collect samples from walls characterized by a complex sequence of render mortars: since their belonging to the different construction and restoration phases of the Church are not always clear, it was decided to distinguish between inner and outer layers of plaster.

The mortars can be distinguished based on their function into bedding, grouting, render and in-fill mortars (Figure 4) [46].

All the samples were studied using a multi-analytical approach. Thin sections of the mortar-based materials were examined via polarized optical microscopy (POM) using an AxioScope A1 microscope (Carl Zeiss, Jena, Germany) at various magnifications, equipped with video camera, 5 Megapixel resolution and AxioVision (V1) image analysis software. It allows us to identify the most important aspects of binders, including their texture (micritic, microsparitic and sparitic) and microstructure (homogeneous or non-homogeneous, etc.), as well as possible recrystallizations and reactions with the aggregates (e.g., with the presence of neoformation phases). Regarding the aggregates, POM provides an initial evaluation of their types, average grain size, grain size distribution and shape in addition to the binder/aggregate ratio (B/A) and porosity [4,47].

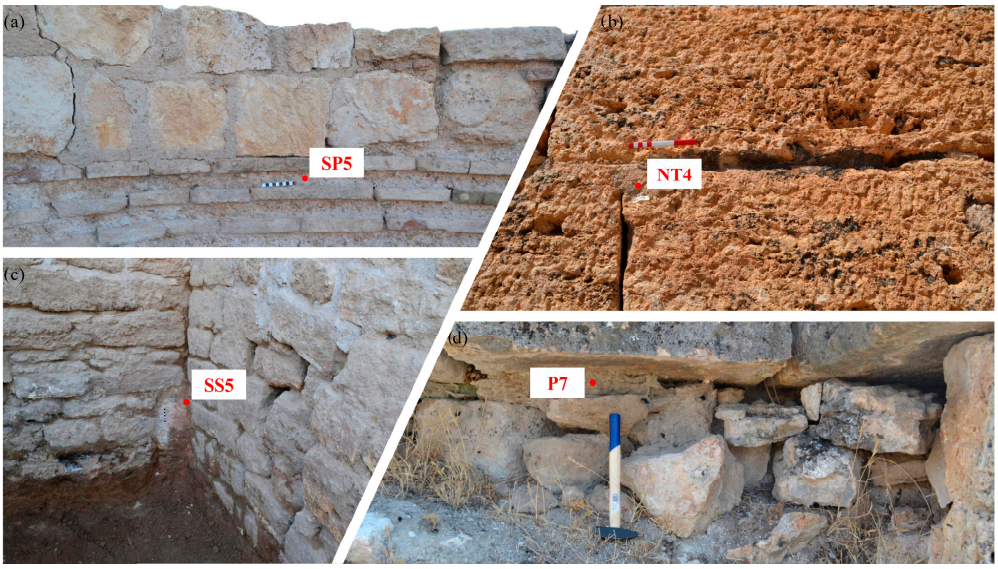

Figure 4. Some examples of (**a**) bedding mortar (SP5 sample—Church of St. Philip); (**b**) grouting mortar (NT4 sample—Nymphaeum of the Tritons); (**c**) coating mortar (SS5—Stoa of the Springs); and (**d**) concrete fill (P7 sample—Ploutonion).

For selected samples, the digital image analysis (DIA) was performed on high-resolution micro-photographs using ImageJ software V1.53t Java 1.8.0.345. This method provides more accurate morphological data on aggregates, including the shape descriptor parameters such as circularity, roundness and aspect ratio, as well as the percentages of each type of aggregate to determine the modal analysis of the mortars. This software makes it possible to automatically determine the B/A ratio, the Feret diameter, the circularity ($C = 4\ \pi A/(P^2)$, where A is the area of the particle and P is the perimeter of the particle), the roundness ($R = 4A/(\pi\ (\text{major axis}^2))$ and the aspect ratio (AR = major axis/minor axis).

The mineralogical composition of bulk mortar powdered samples was performed using X-ray Powder Diffraction (XRPD) using a X'Pert Pro PANalytical diffractometer equipped with an X'Celerator detector (Malvern Panalytical Ltd., Malvern, United Kingdom), with Cu X-ray tube (λ = 1.54 Å), and a Ni-filtered Cu Kα radiation source. The diffraction patterns were recorded under the following conditions: current intensity of 30 mA, voltage of 40 kV, an explored 2θ range of 3–70°, step size of 0.02° and a total time per pattern of 16 min and 27 s. The X'Pert HighScore program and the ICCD database were utilized to identify the mineralogical phases.

The microstructural and semi-quantitative chemical analyses of the polished thin sections were performed using a SEM–EDS (ZEISS EVO MA 15, Oxford Instruments, Abingdon, UK) with W filament equipped with an energy dispersion EDS/SDD analysis system, Oxford Ultimax 40 (40 mm² with a resolution of 127 eV @5.9 keV) with Aztec 5.0 SP1 software. Binders, aggregates and lumps were analyzed under the following conditions: acceleration potential of 15 kV, 500 pA beam current, working distance between 9 and 8.5 mm, 20 s live time as acquisition rate to archive at least 600,000 cts, to Co standard, process time 4 for point analyses, 500 µs pixel dwell time to acquire maps with a resolution of 1024 × 768 pixels. The program used for the microanalysis was an Aztec 5.0 SP1 software using the XPP matrix correction scheme developed by Pouchou and Pichoir in 1991 [48].

3. Results

The results of all analyzed mortar samples are presented here, grouped by function (bedding mortars, opus sectile bedding mortars, grouting mortars, render mortars and in-fill mortars) and age (from the Julio-Claudian to the Middle Byzantine period). This grouping is useful to show possible changes in material provenance and mix design over time.

3.1. Polarized Optical Microscopy (POM)

Table S1 reports the description of the petrographic characteristics of all mortar samples. The samples were listed by function and chronology.

3.1.1. Bedding Mortars

The binders of Roman bedding mortars predominantly exhibit a non-homogeneous appearance, while the Byzantine bedding mortars have a more homogeneous aspect. Textures ranging from micritic to microsparitic (e.g., P1, P2 and SA-C1) (Figure 5a,b,d) are observed for Roman and Byzantine ones. Some samples show partial recrystallization (e.g., SA-A4 and SA-C2) (Figure 5c). The analysis of lumps referred to underburned fragments of stone used for the production of lime suggests that binders were produced by burning travertines (Figure 5e,f) (e.g., P2, P3, TH1 and GB2) and marbles for Roman bedding mortars (Figure 5g,h) (e.g., P1, GB1 and SA-A3). For Byzantine bedding mortars, underburned fragments of marble are more common (e.g., SP16, SP7, SP1, SP2, SP8, SP4 and SP6).

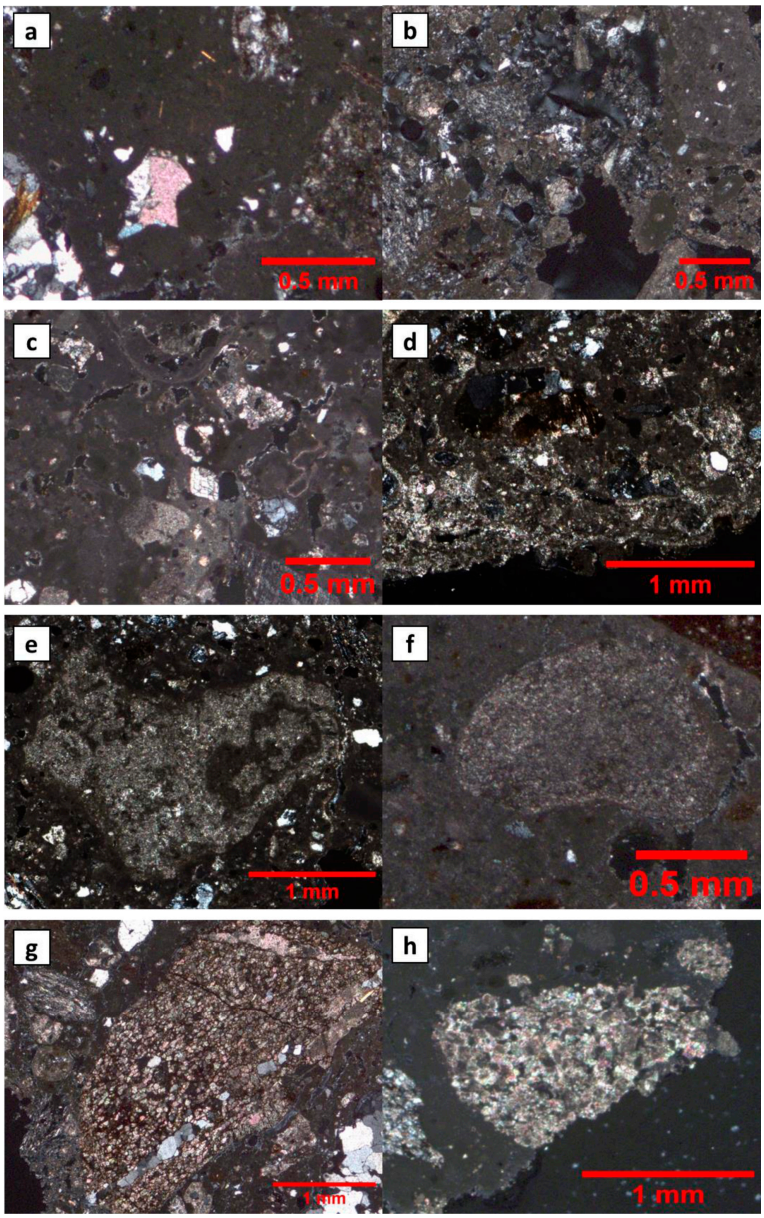

Figure 5. Microphotographs of main aspects of binder and lumps in analyzed mortars (cross polarized nicols): (**a**) SA-C1 homogeneous micritic binder; (**b**) SS7 non-homogeneous binder; (**c**) NA3 binder with

recrystallization; (**d**) P2 binder heterogeneous from micritic to sparitic; (**e**) P2 travertine underburned fragment; (**f**) GB2 travertine underburned fragment; (**g**) P1 marble underburned fragment; (**h**) SP29 marble underburned fragment.

The aggregate of all bedding mortars consists of sedimentary and metamorphic rocks. The sedimentary aggregates are composed of limestones varying from micritic to microsparitic, micritic fossiliferous limestones, travertines and carbonate-cemented breccias containing both sedimentary and metamorphic clasts. Metamorphic rocks are represented by quartzites, phyllites, meta-sandstones, schists, calc-schists, marble, gneiss and amphibolites. Some samples (e.g., SA-A1 and SA-A2) featured ophiolitic aggregates showing either serpentines or mafic holocrystalline gabbro-like rocks.

In Figure 6, the most common types of aggregate are reported.

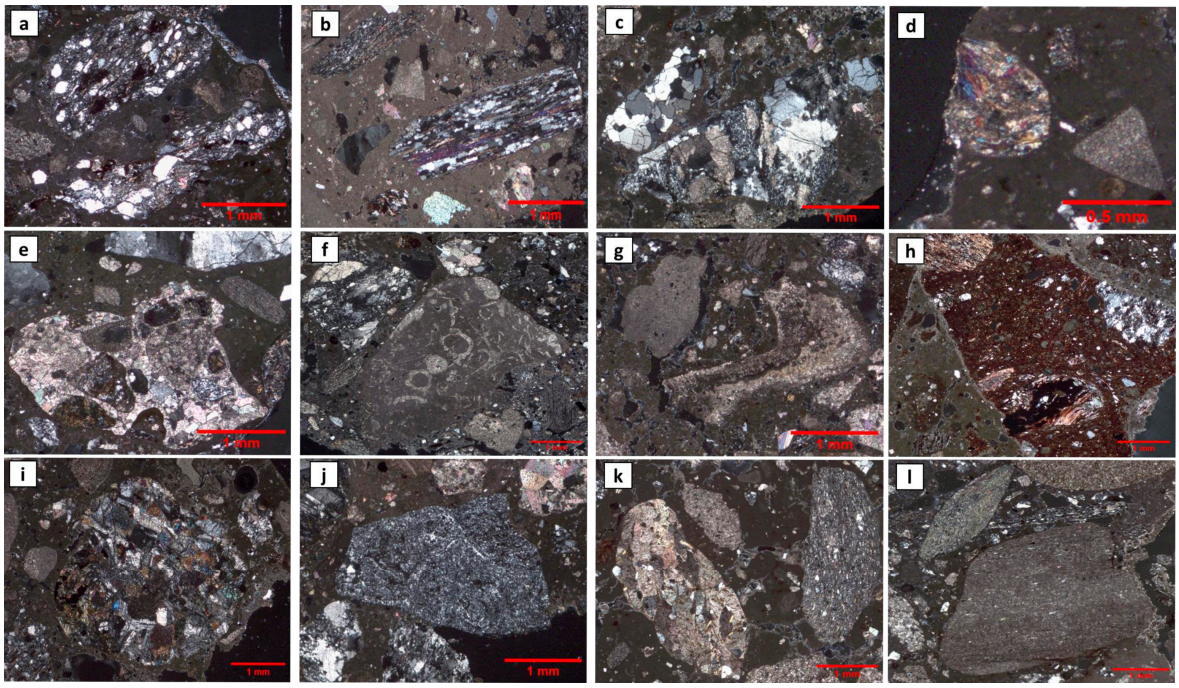

Figure 6. Microphotographs of most common aggregate in analyzed mortars (crossed polarized nicols): (**a**) TH2 gneiss; (**b**) SS7 meta-sandstone and schist; (**c**) SS6 calc-schist and quartzite; (**d**) SA-C1 amphibolite; (**e**) TH2 breccias; (**f**) P6 fossiliferous limestone; (**g**) P1 on the left micritic limestone and on the right travertine; (**h**) SS5 crushed ceramic fragment; (**i**) SA-A2 gabbro-like igneous rock; (**j**) SA-A1 serpentine fragment; (**k**) SS6 marble on the left and schist on the right; (**l**) P6 phyllite with schists.

Most of the bedding mortars show medium porosity. Roman mortars present B/A ratios in the range of 1/1–1/2 to 1/3–1/4 (Figure 7a), while Byzantine ones are in the range of 1/3 and 1/4 (except SP8 with B/A 1/2). Five Roman bedding mortar samples (GB2, TH1, NT1, NT2 and NT3) (Figure 7b) and four Byzantine samples of bedding mortar (SP3, SP5, SP7 and SA-A5) contain aggregate made of crushed ceramic fragments (named *cocciopesto*). This type of aggregate was generally used to confer hydraulic properties to mortars used in water-related contexts [18,49]. It is noteworthy that the temper of the ceramic fragments is very similar to the bedding mortar aggregates. All the samples containing ceramic fragments exhibit medium–low porosity and a different B/A ratio. In particular, B/A ratios of Roman mortars are in the range of 1/1–2/1 and 1/3, while the Byzantine ones show a range of 1/3 and 1/4.

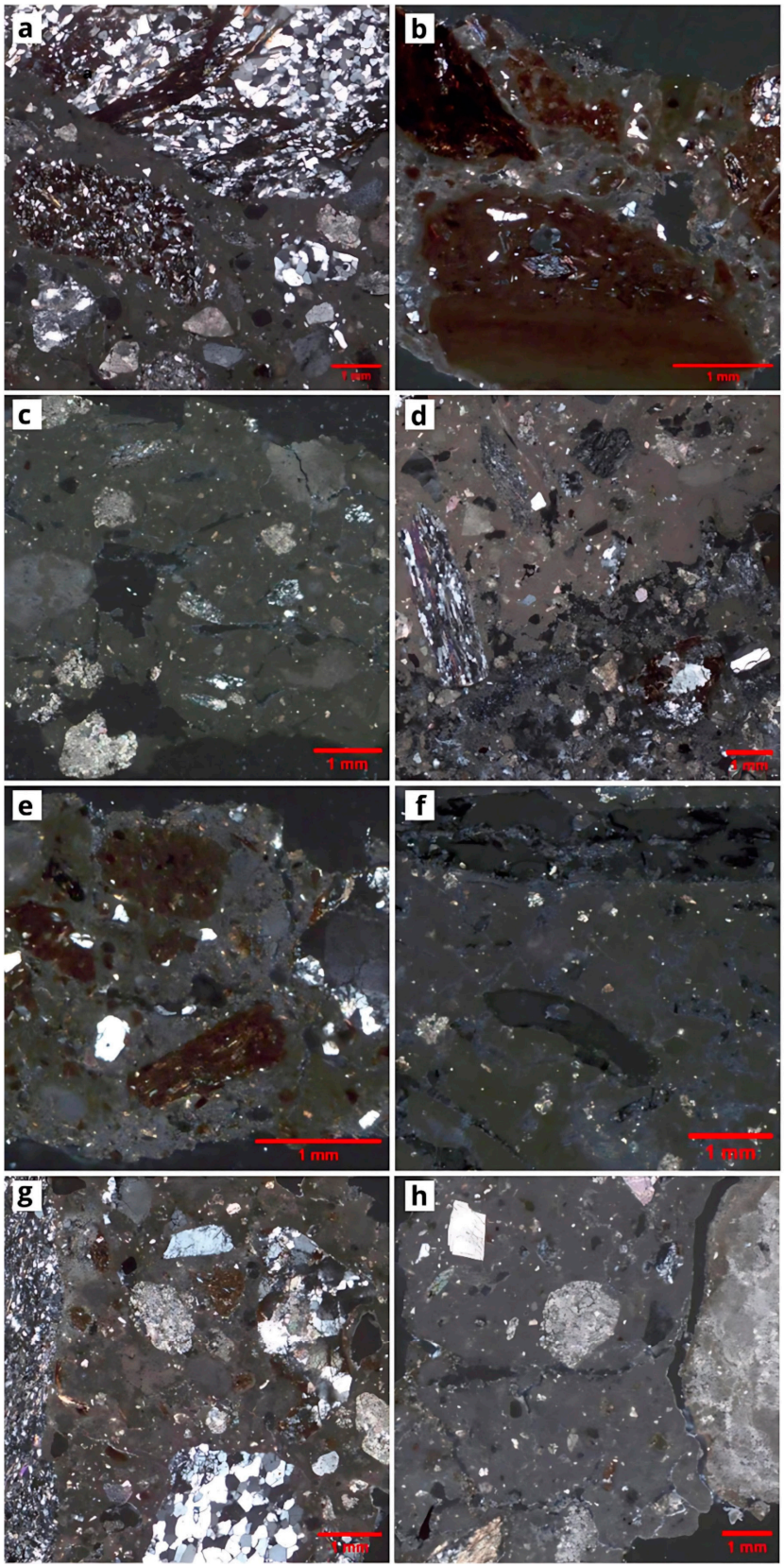

Figure 7. Microphotographs of sample; (**a**) SA-C1 bedding mortar; (**b**) NT1 bedding mortar; (**c**) SP11, render mortar; (**d**) SS7 render mortar; (**e**) SP30 render mortar; (**f**) SP29 render mortar; (**g**) SP36 opus sectile bedding mortar; (**h**) NT4 grouting mortar.

3.1.2. Opus Sectile Bedding Mortars

The opus sectile bedding mortars from the Byzantine St. Philip Church (SP34, SP35, SP36, SP37 and SP38) show various mixing designs that differ due to the content of silicate aggregates and/or carbonate aggregates; however, all the samples, except SP34, contain ceramic fragments.

The aggregate of sample SP34 consists mainly of marble, silicate metamorphic rocks and a smaller number of sedimentary carbonate rocks. Sample SP36 has an aggregate mostly composed of silicate metamorphic rocks and minor quantities of marble and sedimentary limestones with the addition of crushed ceramic fragments (Figure 7g). Samples SP35 and SP38 contain mainly crushed ceramic fragments. SP35 has a small quantity of silicate metamorphic rock fragments, while SP38 contains fragments of carbonate rock. The aggregate of sample SP37 consists of carbonate rock and metamorphic silicate rock fragments with a small number of ceramic fragments. All these opus sectile mortar samples have B/A ratios from 1/2 to 1/3–1/4 and porosity ranging from low to medium.

3.1.3. Grouting Mortars

Both the Roman grouting mortars NT4 and NA2 present micritic binders and aggregates mostly composed of travertine, micritic limestone and marble (Figure 7h). NT4 sample presents a smaller number of carbonate-cemented breccia fragments, quartzites and schists, and sample NA2 shows minor quantities of quartzites and phyllites. Their B/A ratio is in the range from 2/1–3/1 to 1/2–1/3, with porosity from low to medium. The Byzantine grouting mortars, SP32 and SP33, show non-homogeneous binders, B/A ratio 1/3, and medium porosity and different compositions. The aggregates of sample SP32 are mainly ceramic fragments with less n quantities of quartzites and marbles, while mortar SP33 presents mainly ceramic fragments but less quantities of marbles, sedimentary limestones, rare quartzites and gneiss.

3.1.4. Render Mortars

The undated (from 1st century CE to Early Byzantine period) render mortars of the Stoa of the Springs, SS6 and SS7, are characterized by sedimentary and metamorphic rock aggregates but have different features from each other. The SS6 samples has an aggregate made of mostly metamorphic composition, with calc-schists and gneiss as well as a minor qauntity of travertines, ophiolites, marble, quartzites and schists. Its B/A ratio ranged from 1/3 to 1/4 with basically medium porosity. Sample SS7, instead, presents a double layering (Figure 7d). The first layer presents a non-homogeneous binder and aggregates mostly composed of travertine, micritic limestones, marble and quartzites. The second one, covered by a pigmented red layer, shows homogeneous binder and a small number of metamorphic aggregates, mostly meta-sandstones and marble. The coating sample SP9 belongs to a Roman tomb constructed before the St. Philip Church. It presents mostly carbonate aggregates, with a B/A ratio between 1/1 and 2/1. The Early Byzantine inner layers of plasters (SP10, SP11, SP12, SP13, SP14 and SP15) show sedimentary and metamorphic aggregates, with B/A ratios ranging from 1/1 to 1/3–1/4 and with medium porosity. Sample SP11 presents marble and schists, as well as micritic limestones, as aggregate, with B/A ratio 1/1 but high porosity (Figure 7c). On the other hand, all the Early Byzantine outer layers of renders (SP17, SP18, SP19, SP20, SP21, SP22, SP23, SP24, SP25, SP26, SP27, SP28 and SP29) are, almost exclusively, composed of lime and straw and very rare lithic aggregates, with undetermined B/A ratios and very high porosity. In some cases, these mortars present underburned or overburned marble fragments, such as SP29 sample (Figure 7f). Mortar sample SS5, from Stoa of the Springs (Flavian period), has aggregate consisting mainly of ceramic fragments and rare metamorphic silicate rock fragments, with B/A ratio 1/3 and medium porosity. Render mortar NA1 from Nymphaeum of the Apollo Sanctuary (Late Antonine period) contains aggregate mainly of ceramic fragments and less of metamorphic rock fragments. This mortar sample has a B/A ratio of 1/1–2/1 and a medium porosity. The Middle Byzantine renders SP30 and SP31 were found in a former

Roman sarcophagus, later used as a basin in the St. Philip Church, and contain aggregate mainly composed of ceramic fragments with smaller amounts of sedimentary limestone and rare metamorphic rock fragments (Figure 7e). These Byzantine samples have a B/A ratio of 1/3 and low-to-medium porosity.

3.1.5. In-Fill Mortars

The two in-fill samples have different dates. The first one, NA3, used during the Early Byzantine period, has non-homogeneous binder and aggregates mostly composed of metamorphic rocks (calc-schists, schists, marbles, meta-sandstones and phyllites). The B/A ratio is 1/2 with medium porosity. In contrast, the second sample, P7, belonging to the Early Byzantine period, has homogeneous binder with calc-schists, and minor quantities of phyllites, quartzites, meta-sandstones, travertines, micritic limestones and fossiliferous limestones. In this case, the B/A ratio is 1/3–1/4 with medium porosity.

A particular case is represented by sample P8, made of air lime with the addition of crushed marble, belonging to the cladding of a Doric frieze that was re-used in the wall of the northern entrance to the area in front of the grotto of Ploutonion.

3.2. Digital Image Analysis (DIA)

3.2.1. Modal Analysis

The modal analysis of some selected samples, via digital image analysis (DIA), allowed us to determine the percentage of each type of aggregate contained in the mortar. The results are shown in Table S2. The bedding mortars, dating from the Julio-Claudian period to the Flavian period (late 1st century BCE—late 1st century CE), present metamorphic aggregates in the range of 55%–80%, while the content of ophiolitic rocks was less than 5% (as in samples SA-C1, SA-C2, P2, P4, SS1, SS2, SS3, SS4 and GB2). These percentages changed during the Severan period (292–235 CE), with the ophiolitic rock percentage reaching about 17%, and metamorphic aggregates percentage in the range 38%–57% (as in samples of bedding mortars NT1, NT2, NT3, TH1, TH2, SA-A1 and SA-A2), excluding sample SA-A4, whose metamorphic component reached 77%. The metamorphic aggregates are the main component of the Early Byzantine bedding mortars, when ceramic fragments are absent. For instance, sample P6 and sample SP4 contain 74% and 87% of metamorphic aggregates, respectively. Ophiolitic rocks are rarely observed in the Byzantine bedding mortars; indeed, sample P6 and sample SP4 contain ~2.5% and ~1% of ophiolites, respectively (Figure S1). The Middle Byzantine sample SP7 was principally composed of ceramic fragments (88%), so all the other aggregate percentages are very low. This is a common characteristic of all mortars containing ceramic fragments in the range of 83%–98%. The only exception is the Flavian sample GB2, which presents about the same percentages of ceramic fragments and metamorphic aggregates, 42% and 55%, respectively. Concerning the four coating mortars (SS5 Flavian sample and SP31, SP11 and SP29 Early Byzantine), sample SS5 has a very high content of crushed ceramic fragments (98%), as coating SP31, that contains 84% of crushed ceramic fragments. Sample SP11, lacking ceramic fragments, is rich in metamorphic aggregates (81%). Sample SP29 proves itself the archetype of the Early Byzantine external plasters, with a prevalence of lime and straw and very few lithic aggregates. The grouting mortar samples NT4 and SP33, dating from the Severan period and Early Byzantine period, respectively, show different compositions. The aggregate of NT4 is composed of 66% sedimentary rocks (travertine and limestone) with less amount of marble (17%). Sample SP33 presents mainly ceramic fragments as aggregates (81%), with minor quantities of metamorphic rocks (~14%). The Early Byzantine concrete fill sample NA3 has the highest content of metamorphic aggregates (93%), mainly composed of calc-schist, schist and marble.

3.2.2. Shape Factors of Aggregates

The morphological features of each type of aggregate are described in Table S3. After identifying rock types and ceramic fragments in the aggregate of selected mortar sam-

ples, DIA was used to determine the shape factors of the grains of aggregate. The factors evaluated include circularity, Feret diameter, Feret minimum diameter, aspect ratio and roundness. The results, presented in Table S2, demonstrate that the individual lithic components of aggregates and ceramic fragments in the analyzed mortars exhibit morphological characteristics that are more or less constant over time. However, there are some notable exceptions related to the Early Byzantine period. Mortars P6 and SA-A5 from Ploutonion and Sanctuary of Apollo, respectively, contain gabbro-like rocks with aspect ratio (AR) between 3.07 and 3.30, while similar rocks from other periods show AR about 1.5. Additionally, the gabbro-like rocks contained in P6 and SA-A5 show much lower circularity (C = 0.40) compared to circularity of the gabbro-like rocks from other periods (C = 0.65–0.70). Regarding the Early Byzantine mortars from St. Philip Church, all the rock types of aggregate show low circularity values (0.28–0.55).

When we move on to the morphometrical and morphological analysis of the whole thin sections in which many different components are present, the composition of the mortar mixture does not come into play. The average shape factors of the whole sections ignore the variability of the aggregates and are only calculated on the basis of the shapes of all the aggregates without considering their types.

3.2.3. Average Shape Factors of Samples

The average shape factors of the samples are shown in Figure S2.

The aggregates were analyzed with DIA, and the results show that the average shape factors and size of the particles varied over time. Until the end of the Flavian period, the aggregate of all mortars has an average diameter of about one millimeter. This value decreases to about 0.6 mm by the end of the Severan period, with the exception of two outliers from the Severan period (sample NT3 and sample SA A4).

In the Early Byzantine period, the diameter of the aggregate of bedding mortars from the Ploutonion and the Sanctuary of Apollo rises to over 1 mm, while in St. Philip's Church, it decreases to 0.7–0.8 mm. Renders and grouting mortars, belonging to the Early Byzantine period, show a finer aggregate (0.4–0.5 mm).

The average circularity values also show differences among the studied periods. The mortars from the Julio-Claudian period show the lowest average value for circularity (~0.44); this value increases until the end of the Flavian period (0.57). The average circularity value is constant during the Severan period (0.57) and decreases in the Early Byzantine and Middle Byzantine mortars of St. Philip's Church (~0.48). In contrast, the Early Byzantine mortars from the Ploutonion and the Sanctuary of Apollo show a high average circularity (0.61) (Figure S2).

3.3. X-Ray Powder Diffraction (XRPD)

Table 1 (a) and (b) summarize the main mineralogical composition (for abbreviation see [50,51]) of all analyzed mortars.

The mineralogical characterization of the Roman (Table 1 (a)) and Byzantine (Table 1 (b)) mortar samples shows that calcite is the most detected mineralogical phase, followed by quartz and muscovite. Dolomite, which is probably associated with sedimentary limestone fragments [45], occurs in all bedding mortars up to the Flavian period, except for mortar SS1. In the following periods, dolomite was present in three bedding mortars of the Severan period (SA-A4, SA-A1 and SA-A3). In Early Byzantine bedding mortars, dolomite is present in P6 and SP16, and in traces in SP7, SP1, SP8 and SP17. Chlorite was found in all Early Byzantine bedding mortars, except for sample SP3, while chlorite was only rarely present in mortars from other periods (P4, P5, P1, SS2 and P6). Both sample TH2 (Roman period) and sample SP1 (Byzantine period) contained vaterite. This is a crystalline polymorph of calcium carbonate [52,53], which is a metastable compound [4]. Some samples contained gypsum, a mineral phase associated with the sulfation of calcite [54,55]. The bedding mortar NT1 contained whewellite ($CaC_2O_4 \cdot H_2O$), a hydrated calcium oxalate probably caused by hydrothermal alteration [56,57].

Table 1. (**a**) Main mineralogical composition of Roman mortars; (**b**) main mineralogical composition in Byzantine mortars (semiquantitative data, +++: very abundant; ++: abundant; +: present; tr: traces; -: below detection limit).

(a)							
SAMPLE	**Cal**	**Dol**	**Ms**	**Chl**	**Px**	**Qz**	**Others**
Roman bedding mortars							
SA-C1	+++	tr	+	tr	-	++	
SA-C2	++	+	tr	tr	-	+++	
P1	+++	+	+	tr	tr En	++	
P2	+++	+	tr	-	-	+	Arg
P3	+++	+	tr	-	-	+	Arg
P4	++	+	tr	tr	tr Cen, Pgt	+++	Hem
P5	++	++	tr	tr	-	+++	
SS1	+++	-	tr	-	tr En	+	CM
SS2	++	tr	+	tr	-	+++	
SS3	+++	+	tr	-	-	++	
GB1	++	tr	+	-	-	+++	
GB2	+++	tr	tr	-	+ Pgt	++	
TH1	+++	-	tr	-	+ Di	++	CM, Gp
TH2	+++	-	-	-	tr Di, Hd	++	Vtr
NT1	++	-	tr	-	tr Di, Gh	+++	Whe, Pl, Gp
NT2	+++	-	tr	-	tr Di	++	Gp
NT3	+++	-	+	-	tr Di, Gh	++	
SA-A1	+++	-	tr	tr	-	+	Pl
SA-A2	+++	+	tr	tr	-	++	Pl
SA-A3	+++	tr	+	tr	-	++	Pl
SA-A4	+++	+	tr	-	-	+	
P6	+++	+	+	tr	-	++	
SA-A5	+++	-	+	-	tr Di	++	Hem
Roman render mortars—external							
SP9	+++	+	+	tr	-	++	
SS5	+++	-	+	tr Di	-	++	
Roman grouting mortars							
NA2	+++	tr	tr	-	tr Cen	++	Gp
NT4	+++	-	+	tr	-	++	
Roman ceramic-rich render							
NA1	+++	-	tr	-	+ Di, Gh	++	
Marmorino cladding in Ploutonion							
P8	+++	+	-	-	-	-	Arg, Gp
Uncertain dated Stoa of the Springs renders							
SS6	+++	+	+	tr	-	++	
SS7	+++	-	-	-	-	++	CM, Gp

Table 1. *Cont.*

(b)							
SAMPLE	**Cal**	**Dol**	**Ms**	**Chl**	**Px**	**Qz**	**Others**
Byzantine bedding mortars							
SP1	+++	tr	tr	+	-	++	Vtr
SP2	+++	-	tr	tr	-	++	Ank
SP3	+++	-	tr	-	+ Di, Gh	++	Pl
SP4	+++	-	+	tr	-	++	CM
SP5	++	-	+	tr	tr Di, Gh	+++	Crd, Gp
SP6	+++	tr	+	tr	-	++	
SP7	+++	tr	-	-	-	tr	
SP8	+++	tr	tr	-	-	++	CM, Crd
Byzantine render mortars—inner layer							
SP10	+++	tr	tr	tr	-	+	
SP11	+++	+	tr	-	-	+	Gp
SP12	+++	+	tr	-	-	++	CM
SP13	+++	+	tr	tr	-	++	Crd
SP14	+++	tr	tr	-	-	+	
SP15	+++	+	tr	tr	-	+	
Byzantine render mortars—external layer							
SP16	+++	+	tr	+	-	++	Gp
SP17	+++	-	-	-	-	tr	Kfs, Gp
SP18	+++	-	-	-	-	tr	Pl, Gp
SP19	+++	-	-	-	-	+	Gp
SP20	+++	-	+	-	-	+	
SP21	+++	-	-	-	-	tr	
SP22	+++	-	-	-	-	tr	
SP23	+++	-	-	-	-	+	
SP24	+++	-	tr	tr	-	+	Arg
SP25	+++	+	-	-	-	+	Gp
SP26	+++	-	-	-	-	+	
SP27	+++	-	-	-	-	+	Arg
SP28	+++	tr	tr	tr	-	+	Gp
SP29	+++	-	tr	-	-	+	
Byzantine opus sectile bedding mortars							
SP34	+++	tr	+	-	-	++	Gp
SP35	+++	-	+	tr	tr Di, Gh	++	Hem
SP36	+++	-	+	-	tr Di, Gh	++	
SP37	+++	+	+	-	tr Di, Gh	++	Gp
SP38	+++	-	+	-	+ Di, Gh	++	
Byzantine grouting mortars							
SP32	+++	-	+	tr	+ Di, Gh	++	
SP33	+++	-	+	-	+ Di, Gh	++	

Table 1. *Cont.*

(b)							
SAMPLE	**Cal**	**Dol**	**Ms**	**Chl**	**Px**	**Qz**	**Others**
Byzantine ceramic-rich renders							
SP30	++	-	tr	-	+ Di, Gh	+++	
SP31	+++	-	+	-	tr Di	++	
Byzantine in-fill mortar							
NA3	++	-	tr	tr	+Cen	+++	
P7	+++	-	+	tr	-	++	

Abbreviation legend: Cal = calcite; Dol = dolomite; Arg = aragonite; Vtr = vaterite; Whe = whewellite; Gp = gypsum; Ms = muscovite; Chl = chlorite; Px = pyroxene (En = enstatite, Cen = clinoenstatite, Pgt = pigeonite, Di = diopside, Gh = gehlenite, Hd = hedengergite); Qz = quartz; Hem = hematite; Pl = plagioclase; Crd = cordierite; Kfs = K-feldspar; Ank = ankerite; CM = clay minerals. Abbreviations from [50,51].

The XRPD analysis of the coating and plaster samples shows that calcite is the most important mineral phase, followed by the presence of quartz. The Roman coatings and the Early Byzantine inner layers of plasters from the St. Philip Church contain traces of muscovite or other phyllosilicates, but these mineral phases are rarely observed in the Byzantine external layers of plaster. Some Byzantine external layers of plaster show few mineral phases in X-ray diffraction patterns, which are characterized by the presence of calcite with a small amount of quartz. The Early Byzantine inner plasters contain dolomite, while this mineral is rare in the Byzantine external plasters and in the Roman coatings. Several samples contain gypsum from alteration; the external plaster SP17 shows traces of vaterite; probably vaterite is present in the samples from Hierapolis as an alteration phase due to the hydrothermal environment [52,58]. Regardless of function and age, most mortar-based materials containing ceramic fragments in the aggregate have pyroxenes, especially diopside and/or gehlenite. These are probably related to the firing of the ceramic [59,60]. In the mortar samples containing lithic aggregates, we note that the pyroxenes, when present, are mainly composed of clinoenstatite and/or enstatite. In this case, these pyroxene compositions can be associated with the presence of ophiolitic rock fragments. The main mineralogical phase of all the grouting samples is calcite, followed by muscovite and abundant quartz. The Early Byzantine grouting mortars contain diopside and gehlenite, which are absent in the Roman grouting samples, NA2 has enstatite and NT4 is pyroxene-free. As for the Byzantine opus sectile mortars, we note the usual presence of calcite and quartz. The mortar samples SP35, SP36, SP37 and SP38, which contain crushed ceramic fragments as aggregates, show diopside and/or gehlenite, and SP35 has traces of hematite.

3.4. Scanning Electron Microscope/Energy Dispersive Spectroscopy

Microchemical and morphological SEM–EDS studies were conducted to further investigate the properties of binder and lumps. Representative samples were selected based on construction phase, function, POM and DIA characteristics. The binder characteristics of samples are variable and can be represented into two main types: mortars with a heterogeneous micritic binder and *cocciopesto* aggregates (NT2, SS5, SP31 and SP33); mortars with a homogeneous micritic binder (P7) or a non-homogeneous micritic/microsparitic binder (SA-A1 and SA-C1) and lithic aggregates. These samples were analyzed to investigate hydraulic behavior, the presence of reaction rims and Mg content. The hydraulicity index (HI) [61] was calculated based on chemical data obtained via SEM–EDS analysis of the binder, lumps and reaction rims (Figure 8). The chemical data collected from the unburned fragments of the stone used for lime allowed us to identify the composition of the carbonate rock utilized. Figure 8d presents the calculated HI values based on at least 15 measurements taken on the binder and lumps for each sample (Table S4). The role of ceramic fragments

was investigated using HI values, which ranged from 0.04 to 0.10 in the lime lumps and from 0.15 to 0.30 in the binder/reaction rim. Mortars containing ceramic fragments can be classified as weak-to-moderate hydraulic binder. The backscattered image (BSE) of samples NT2 and SS5 shows reaction rims between the binder and the ceramic fragments (Figure 8a,c). Mortars with a heterogeneous/homogeneous micritic/microsparitic binder and lithic aggregates (SA-A1 and SA-C1) can be considered composed of air lime binder, with HI values of 0.04 for the lime lump and 0.03–0.08 for the binder. Sample P7 has a binder with an HI of 0.14, indicating a weak hydraulic mortar. However, the analysis of the underburned lumps shows high Ca values and a variable amount of Si due to the presence of microcrystalline quartz included in the stone used for mortar production (Figure 8d). The HI value could be explained by contamination from the finest aggregate fraction (quartz, underburned during the firing). Based on the underburned fragments found in the mortar samples, the primary source of lime appears to be relatively pure calcium carbonate, excluding rocks containing Mg.

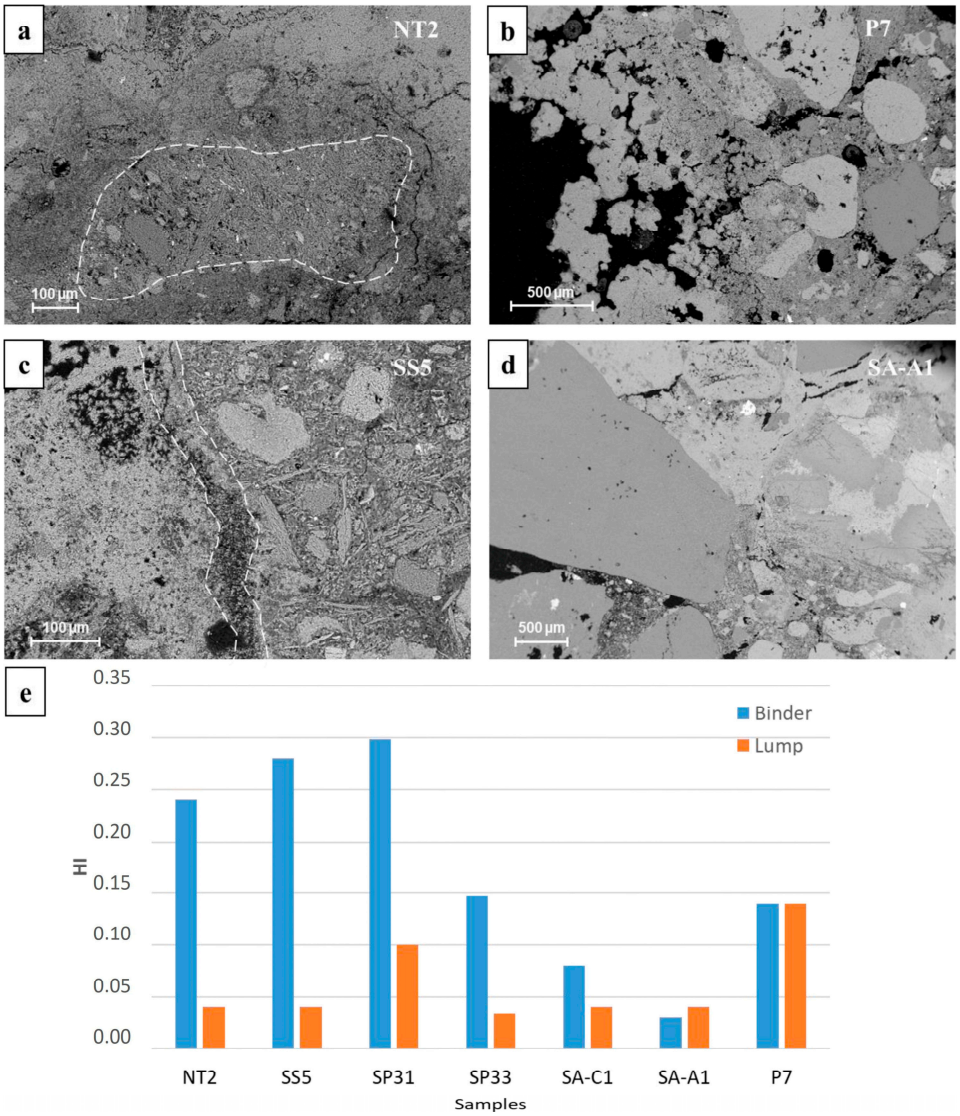

Figure 8. Backscattered SEM image of binder: (**a**,**c**) reaction rim between binder and ceramic fragment (NT2 and SS5, respectively); (**b**,**d**) air lime binder (P7 and SA-A1, respectively); (**e**) HI calculated on selected samples using microchemical SEM–EDS data of binders and lumps. All the acquired data are presented in Table S4.

4. Discussion

4.1. Raw Material Provenance

4.1.1. Binder Raw Materials

The results allow us to hypothesize the sources of the raw materials. In the Roman period, both travertine and marble were used to produce the binders of mortar-based materials. Travertine in particular was easily accessible, as it outcrops near Hierapolis and even forms the plateau on which the city was built [62]. Both white and white-grey marbles were used and quarried in the quarries of Gök Dere and Marmar Tepe, which are located in close proximity to the city center (1–2 km). In addition, quarries a little further away, such as those at Thiounta and Gölemezli, were also exploited [63]. In the Early Byzantine period, the use of marble as stone for lime became very common, probably due to the reuse of debris from monumental buildings that had collapsed after earthquakes [64,65]. Travertine was no longer used during this period.

4.1.2. Aggregate Raw Materials

All the analyzed samples contain different types of aggregates of sedimentary and/or metamorphic origin with grain morphologies compatible with the fluvial sediments such as sands and gravels. The lithologies of the aggregates correspond to rocks eroded by the watercourses. Not far from the city, small watercourses such as Gök Dere, Kadı Dere and Suini Dere carry fragments of metamorphic rocks such as quartzites, schists, marble, gneiss, meta-sandstones and phyllites associated with the Menderes Massif [33]. The erosion of rocks that outcrop directly on the terrace on which the city of Hierapolis is located produces fragments of travertine and, more rarely, of carbonate-cemented breccias. The aggregates such as sedimentary limestones and ophiolites are derived from the Lycian Nappe units that outcrop in the part of the basin dominated by Mount Honaz on the south/southwest side of the Denizli Basin. These lithologies are eroded and entrained by tributaries of the Çürüksu River, such as the Gökpınar stream and the Alikurt creek. The same type of lithologies outcrop west of Hierapolis, where they can be carried by the Saraçay stream a tributary of the Çürüksu (see Figure 2b). The XRPD analysis shows that the pyroxenes present in all the mortars containing crushed ceramic fragments are mainly diopside and gehlenite, probably formed during the firing of carbonate clay for the pottery production at temperatures between 550 and 950 °C [66]. It is worth mentioning that the ceramic fragments could belong to local pottery or tiles due to their composition, which consists of both siliceous metamorphic rock fragments (schist, quartzite and gneiss) and still-recognizable carbonate rock fragments (marble and sedimentary carbonates). For the different historical periods, the image analysis of the mortar-based materials shows differences in both sedimentary and metamorphic aggregates in terms of average shape parameters (especially average circularity), proportions of the used rock types and grain size. This evidence could indicate the use of raw materials from different sources (e.g., sediments from different rivers) or different mortar production technologies with the use of skills such as sieving or grinding of aggregates. The simultaneous decrease in the average size and the average circularity of the aggregate grains suggests a possible grinding process of the rocks, which influences both parameters and produces finer and more irregular grains. Sieving, on the other hand, changes the average size but has no effect on the average circularity of the aggregate grains. Specifically, all the mortars examined from the Flavian to the Severan periods show changes in the proportion of metamorphic and sedimentary rocks, which are accompanied by a reduction in the average size of the aggregates. The Early Byzantine mortars generally have smaller grain sizes than the mortars of the Severan period, except for the Early Byzantine bedding mortars from the Ploutonion and the Building A in the Apollo Sanctuary. These samples have a larger grain size than the mortars from the same period. This seems to be related to the specific buildings and does not contradict the general trend. In the Early Byzantine mortars from St. Philip Church, aggregates present the most distinctive characteristics in shape and size. Not only the types of rocks used as aggregate have low values of circularity, but the average circularity of these samples is also low, indicating very

angular grains and the grain sizes are very fine, except for the aggregates used in bedding mortars. These peculiar features of the Early Byzantine mortars indicate a different source of raw material and/or a grinding process. In the first case, the watercourse carrying the aggregate (gravels and/or sands) may not have had sufficient flow to round the grains. As for the provenance of the poorly processed sediments, we can assume that they originate from the bed of the Suini Dere, a local seasonal stream, which flows north-east of St. Philip Hill. Changes in the raw material supplies may also be confirmed by the composition of the Early Byzantine mortars from the Ploutonion (P7 and P6), which contain phyllites in their aggregate. This type of rock is also found in samples NA2 (grouting mortar from Late Antonine period) and NA3 (in-fill mortar) belonging to the Nymphaeum of Apollo (Early Byzantine) and in the coating sample SS6 of an uncertain date from the Stoa of the Springs containing phyllite. Phyllite is associated with the low-metamorphic facies of the Menderes Massif. As all samples that contain phyllite are dated Early Byzantine, with an exception (sample NA2), we can hypothesize that this rock is a marker for Early Byzantine masonry in Hierapolis. Based on the presence of phyllite, sample SS6 can be dated to Early Byzantine age, while NA2 could be re-dated and considered coeval with sample SS6. Indeed, this hypothesis is supported by the traces of ancient restoration that occurred to the Nymphaeum, which can be detected also in the masonry technique.

4.1.3. Technological Evidence

The petrographic analysis shows differences in the mix design of the bedding mortars: the Roman bedding mortars containing ceramic fragments as aggregate have $B/A \leq 1/3$; the Byzantine bedding mortars with ceramic fragments as aggregate have prevalently $B/A \geq 1/3$. It is noteworthy that ceramic fragments were repeatedly added during the Roman period to improve the hydraulic properties of mortars in water-related contexts (e.g., Nymphaeum of the Tritons, Stoa of the Springs, the Great Building—Roman Baths). However, this technological ability was not always retained later. Thus, the Early Byzantine samples SP3 and SP5, both from the apse of St. Philip, contain mainly ceramic fragments with no hydraulic function, as do the Early Byzantine grouting mortars SP32 and SP33. These samples consist mainly of ceramic fragments and silicate stone, although they were not intended to fulfill a hydraulic function, which testifies to the progressive loss of certain knowledge over time. A technical feature of the Early Byzantine period is instead the creation of two different mixing designs for the production of plasters (inner layers in the church of St. Philip) and bedding mortars. These mortars of the same age with different functions have different aggregate compositions. For example, the bedding mortars rarely contain dolomite, which is found in all the inner plaster layers. Dolomite is associated with the carbonate rocks of the Lycian Nappe [45], and the presence or absence of this mineral suggests a change in the supply area of raw materials. As for Early Byzantine external layers of plasters, we note that they are composed of lime with the addition of straw, while the use of lithic aggregates is rare. The addition of straw to the mortar and/or plaster mix is a common technique to improve their resistance under certain environmental conditions. In earthquake-prone areas, it is highly desirable to improve the fracture behavior of masonry and make the materials more flexible and lightweight [67,68].

5. Conclusions

The possibility of analyzing a large number of mortar samples with different functions and different dating, combined with an in-depth knowledge of the territory from a geological and geomorphological point of view, allows us to understand the evolution of raw material supply and production technologies in the archaeological site of Hierapolis of Phrygia (Turkey).

Our study confirms that marble and the easily accessible travertine, which is abundant in the region, were the main source of lime in Roman mortar binders. In the Early Byzantine period, marble was used more frequently, probably due to the reuse of rubble from collapsed monumental buildings of the Roman city. Regarding the raw materials used as aggregates,

local travertine and carbonate breccias, as well as fluvial sediments from eroded rocks of the Menderes Massif and the Lycian Nappe, were used in both the Roman and Byzantine periods. We can also assume that the ceramics used in the mortar-based materials were locally produced, as both the mortar mixture and the ceramic fragments contain the same metamorphic rock type. From a technological point of view, while ceramic fragments were consistently used in Roman mortars to improve hydraulic properties, this practice was not uniformly maintained in later periods. Instead, Early Byzantine mortars show a dual approach in their mix designs for the inner layers of plaster and bedding mortars, with specific aggregate compositions tailored to each function. External layers of plasters from this period also show a shift towards the use of lime and straw, while the proportion of lithic aggregates decreased.

Digital image analysis (DIA) has revealed variations in the proportions of composition of the aggregates in the different periods and changes in the morphological features, suggesting different collection areas along the rivers. From morphological evidence, the Early Byzantine mortars in Church of St. Philip have very angular and fine-grained aggregates, suggesting a grinding process. Overall, the use of local raw materials remained a constant factor in mortar production over time, but the differences in aggregate composition and morphological features can indicate shifts in raw material sources and technological knowledge. These results emphasize the dynamic nature of building practices in Hierapolis and provide a framework for future research on historical mortars and their raw material sources.

Supplementary Materials: The following supporting information can be downloaded at https://www.mdpi.com/article/10.3390/min14111143/s1. Table S1: Main petrographic characteristics of all mortar samples. The samples were listed by function and chronology; Table S2: Modal analysis of aggregates of mortar-based materials; Table S3: Morphometric and morphological parameters of aggregates analyzed with digital image analysis. Table S4: Micro-chemical SEM EDS data; Figure S1: Composition of aggregates of bedding mortars; Figure S2: Average shape factors for the aggregates in bedding mortars.

Author Contributions: Conceptualization, E.C. and T.I.; Methodology, E.C., T.I., M.M.N.F. and S.C.; Validation, E.C., S.V. and T.I.; Formal Analysis, M.M.N.F., S.C., E.C. and S.V.; Investigation, M.M.N.F., S.C., E.C. and S.V.; Resources, T.I., M.P.C. and G.S.; Data Curation, M.M.N.F. and S.C.; Writing—Original Draft Preparation, M.M.N.F., S.C., E.C., S.V., M.P.C. and G.S.; Writing—Review and Editing, M.M.N.F., S.C., E.C., S.V., M.P.C. and G.S.; Visualization, M.M.N.F., S.C., E.C., S.V., M.P.C. and G.S.; Supervision, E.C. and T.I. All authors have read and agreed to the published version of the manuscript.

Funding: This research received no external fundings.

Data Availability Statement: All data are available in the manuscript and Supplementary Materials.

Acknowledgments: The authors thank the Centro di Servizi di Microscopia Elettronica e Microanalisi (MEMA), University of Florence, for their kindly assistance in the use of a Scanning Electron Microscope.

Conflicts of Interest: The authors declare no conflicts of interest.

References

1. Franzini, M.; Leoni, L.; Lezzerini, M. A Procedure for Determining the Chemical Composition of Binder and Aggregate in Ancient Mortars: Its Application to Mortars from Some Medieval Buildings in Pisa. *J. Cult. Herit.* **2000**, *1*, 365–373. [CrossRef]
2. Riccardi, M.P.; Lezzerini, M.; Carò, F.; Franzini, M.; Messiga, B. Microtextural and Microchemical Studies of Hydraulic Ancient Mortars: Two Analytical Approaches to Understand Pre-Industrial Technology Processes. *J. Cult. Herit.* **2007**, *8*, 350–360. [CrossRef]
3. Arizzi, A.; Cultrone, G. Mortars and Plasters-How to Characterise Hydraulic Mortars. *Archaeol. Anthropol. Sci.* **2021**, *13*, 144. [CrossRef]
4. Cantisani, E.; Fratini, F.; Pecchioni, E. Optical and Electronic Microscope for Minero-Petrographic and Microchemical Studies of Lime Binders of Ancient Mortars. *Minerals* **2022**, *12*, 41. [CrossRef]

5. Piovesan, R.; Mazzoli, C.; Maritan, L. Production Recipes of Mortar-Based Materials from Ancient Pompeii by Quantitative Image Analysis Approach: The Microstratigraphy of Plasters in the Temple of Venus. *J. Cult. Herit.* **2023**, *59*, 57–68. [CrossRef]
6. Columbu, S.; Garau, A.M.; Lugliè, C. Geochemical characterisation of pozzolanic obsidian glasses used in the ancient mortars of Nora Roman theatre (Sardinia, Italy): Provenance of raw materials and historical–archaeological implications. *Archaeol. Anthropol. Sci.* **2019**, *11*, 2121–2150. [CrossRef]
7. Miriello, D.; Antonelli, F.; Apollaro, C.; Bloise, A.; Bruno, N.; Catalano, M.; Columbu, S.; Crisci, G.M.; De Luca, R.; Lezzerini, M.; et al. A petro-chemical study of ancient mortars from the archaeological site of Kyme (Turkey). *Period. Mineral.* **2015**, *84*, 497–517. [CrossRef]
8. Lezzerini, M.; Ramacciotti, M.; Cantini, F.; Fatighenti, B.; Antonelli, F.; Pecchioni, E.; Fratini, F.; Cantisani, E.; Giamello, M. Archaeometric Study of Natural Hydraulic Mortars: The Case of the Late Roman Villa dell'Oratorio (Florence, Italy). *Archaeol. Anthropol. Sci.* **2017**, *9*, 603–615. [CrossRef]
9. Boese, B.; Amicone, S.; Cantisani, E.; Schön, F. Mortars in Context: An Integrated Study of Mortars and Plasters from the So-Called Ginnasio in Solunto (Sicily, Italy). *Archaeometry* **2023**, *65*, 702–720. [CrossRef]
10. Dilaria, S.; Secco, M.; Ghiotto, A.R.; Furlan, G.; Giovanardi, T.; Zorzi, F.; Bonetto, J. Early Exploitation of Neapolitan Pozzolan (Pulvis Puteolana) in the Roman Theatre of Aquileia, Northern Italy. *Sci. Rep.* **2023**, *13*, 30692. [CrossRef]
11. Anania, L.; Badalà, A. Mechanical Properties and Durability of Ancient Mortars in the Historic Buildings of Eastern Sicily. *Mech. Adv. Mater. Struct.* **2022**, *29*, 372–383. [CrossRef]
12. Miriello, D.; Barca, D.; Bloise, A.; Ciarallo, A.; Crisci, G.M.; De Rose, T.; Gattuso, C.; Gazineo, F.; La Russa, M.F. Characterisation of Archaeological Mortars from Pompeii (Campania, Italy) and Identification of Construction Phases by Compositional Data Analysis. *J. Archaeol. Sci.* **2010**, *37*, 2207–2223. [CrossRef]
13. Miriello, D.; Bloise, A.; Crisci, G.M.; De Luca, R.; De Nigris, B.; Martellone, A.; Osanna, M.; Pace, R.; Pecci, A.; Ruggieri, N. New Compositional Data on Ancient Mortars and Plasters from Pompeii (Campania—Southern Italy): Archaeometric Results and Considerations about Their Time Evolution. *Mater. Charact.* **2018**, *146*, 189–203. [CrossRef]
14. Secco, M.; Previato, C.; Addis, A.; Zago, G.; Kamsteeg, A.; Dilaria, S.; Canovaro, C.; Artioli, G.; Bonetto, J. Mineralogical Clustering of the Structural Mortars from the Sarno Baths, Pompeii: A Tool to Interpret Construction Techniques and Relative Chronologies. *J. Cult. Herit.* **2019**, *40*, 265–273. [CrossRef]
15. Rispoli, C.; Graziano, S.F.; Di Benedetto, C.; De Bonis, A.; Guarino, V.; Esposito, R.; Morra, V.; Cappelletti, P. New Insights of Historical Mortars Beyond Pompeii: The Example of Villa Del Pezzolo, Sorrento Peninsula. *Minerals* **2019**, *9*, 575. [CrossRef]
16. Dilaria, S.; Previato, C.; Secco, M.; Busana, M.S.; Bonetto, J.; Cappellato, J.; Ricci, G.; Artioli, G.; Tan, P. Phasing the History of Ancient Buildings through PCA on Mortars' Mineralogical Profiles: The Example of the Sarno Baths (Pompeii). *Archaeometry* **2022**, *64*, 866–882. [CrossRef]
17. Marra, F.; D'Ambrosio, E.; Gaeta, M.; Monterroso-Checa, A. Petrographical and Geochemical Criteria for a Chronology of Roman Mortars between the First Century BCE and the Second Century CE: The Curia of Pompey the Great. *Archaeometry* **2022**, *64*, 597–610. [CrossRef]
18. Rispoli, C.; Montesano, G.; Verde, M.; Morra, V.; Cappelletti, P. The key to ancient Roman mortars hydraulicity: Ceramic fragments or volcanic materials? A lesson from the Phlegrean archaeological area (southern Italy). *Constr. Build. Mater.* **2024**, *411*, 134408. [CrossRef]
19. Kumsar, H.; Aydan, Ö.; Şimşek, C.; D'Andria, F. Historical Earthquakes That Damaged Hierapolis and Laodikeia Antique Cities and Their Implications for Earthquake Potential of Denizli Basin in Western Turkey. *Bull. Eng. Geol. Environ.* **2016**, *75*, 519–536. [CrossRef]
20. Arthur, P. Hierapolis Bizantina e Turca (Pamukkale). In *Guida Archeologica*; Ege Yayinlari: Istanbul, Turkey, 2006.
21. D'Andria, F. *Hierapolis di Frigia (Pamukkale)*; Ege Yayınları: Istanbul, Turkey, 2003.
22. Scardozzi, G. Nuovo Atlante di Hierapolis di Frigia. In *Cartografia Archeologica Della Città e delle Necropoli*; Ege Yayınları: Istanbul, Turkey, 2015.
23. Van Hinsbergen, D.J.J.; Kaymakci, N.; Spakman, W.; Torsvik, T.H. Reconciling the Geological History of Western Turkey with Plate Circuits and Mantle Tomography. *Earth Planet. Sci. Lett.* **2010**, *297*, 674–686. [CrossRef]
24. Gökgöz, A.; Yilmazli, I.E.; Gungor, I.; Yavuzer, I. Hydrogeology and Environmental Study at the Karahayit Geothermal Field (Western Turkey). In Proceedings of the World Geothermal Congress 2010, Bali, Indonesia, 25–29 April 2010.
25. Altunel, E.; Hancock, P.L. Morphology and Structural Setting of Quaternary Travertines at Pamukkale, Turkey. *Geol. J.* **1993**, *28*, 335–346. [CrossRef]
26. Şimşek, Ö.; Günay, G.; Elhatip, H.; Ekmekçi, M. Environmental Protection of Geothermal Waters and Travertines at Pamukkale, Turkey. *Geothermics* **2000**, *29*, 557–572. [CrossRef]
27. Özkul, M.; Varol, B.; Alçiçek, M.C. Depositional Environments and Petrography of Denizli Travertines. *Bull. Miner. Res. Explor.* **2002**, *125*, 13–29.
28. Kele, S.; Özkul, M.; Fórizs, I.; Gökgöz, A.; Baykara, M.O.; Alçiçek, M.C.; Németh, T. Stable Isotope Geochemical Study of Pamukkale Travertines: New Evidences of Low-Temperature Non-Equilibrium Calcite-Water Fractionation. *Sediment. Geol.* **2011**, *238*, 191–212. [CrossRef]
29. Özler, H.M. Hydrogeology and Geochemistry in the Curuksu (Denizli) Hydrothermal Field, Western Turkey. *Environ. Geol.* **2000**, *39*, 1169–1180. [CrossRef]

30. Şimşek, Ö. Hydrogeological and Isotopic Survey of Geothermal Fields in the Buyuk Menderes Graben, Turkey. *Geothermics* **2003**, *32*, 669–678. [CrossRef]
31. Van Noten, K.; Topal, S.; Baykara, M.O.; Özkul, M.; Claes, H.; Aratman, C.; Swennen, R. Pleistocene-Holocene Tectonic Reconstruction of the Ball?k Travertine (Denizli Graben, SW Turkey): (De)Formation of Large Travertine Geobodies at Intersecting Grabens. *J. Struct. Geol.* **2019**, *118*, 114–134. [CrossRef]
32. Shukla, M.K.; Sharma, A. A Brief Review on Breccia: Its Contrasting Origin and Diagnostic Signatures. *Solid Earth Sci.* **2018**, *3*, 50–59. [CrossRef]
33. Cantisani, E.; Vettori, S.; Ismaelli, T.; Scardozzi, G. Imperial Age Mortars at Hierapolis: Raw Materials and Technologies. In *Ancient Quarries and Building Sites in Asia Minor. Research on Hierapolis in Phrygia and Other Cities in South-Western Anatolia: Archaeology, Archaeometry, Conservation*; Ismaelli, T., Scardozzi, G., Eds.; Edipuglia: Bari, Italy, 2017. [CrossRef]
34. Brilli, M.; Conte, A.M.; Giustini, F.; Pilar Lapuente Mercadal, M.; Melica, D.; Quarta, G.; Royo Plumed, H.; Scardozzi, G. Archaeometric Characterization of the White Marbles from the Ancient Quarries in the Territory of Hierapolis and in the Southern Sector of the Denizli Basin, with an Appendix on the Aphrodisian Marble. In *Ancient Quarries and Building Sites in Asia Minor: Research on Hierapolis in Phrygia and Other Cities in South-Western Anatolia: Archaeology, Archaeometry, Conservation*; Ismaelli, T., Scardozzi, G., Eds.; Edipuglia: Bari, Italy, 2017. [CrossRef]
35. Scardozzi, G. The Provenance of Marbles and Alabasters Used in the Monuments of Hierapolis in Phrygia (Turkey): New Information from a Systematic Review and Integration of Archaeological and Archaeometric Data. *Heritage* **2019**, *2*, 519–552. [CrossRef]
36. Rimmelé, G.; Parra, T.; Goffé, B.; Oberhänsli, R.; Jolivet, L.; Candan, O. Exhumation Paths of High-Pressure-Low-Temperature Metamorphic Rocks from the Lycian Nappes and the Menderes Massif (SW Turkey): A Multi-Equilibrium Approach. *J. Petrol.* **2005**, *46*, 641–669. [CrossRef]
37. Çelik, Ö.F.; Chiaradia, M. Geochemical and Petrological Aspects of Dike Intrusions in the Lycian Ophiolites (SW Turkey): A Case Study for the Dike Emplacement along the Tauride Belt Ophiolites. *Int. J. Earth Sci.* **2008**, *97*, 1151–1164. [CrossRef]
38. Sözbilir, H. Oligo-Miocene Extension in the Lycian Orogen: Evidence from the Lycian Molasse Basin, SW Turkey. *Geodinamica Acta* **2005**, *18*, 255–282. [CrossRef]
39. Şimşek, C. Urban Planning of Laodikeia on the Lykos in the Light of New Evidence. In *Landscape and History in the Lykos Valley: Laodikeia and Hierapolis in Phrygia*; Şimşek, C., D'Andria, F., Eds.; Cambridge Scholars Publishing: Cambridge, UK, 2016; pp. 1–46.
40. Campagna, L.; Scardozzi, G. Archeologia Delle Acque a Hierapolis di Frigia: Tematiche Principali e Metodologie Integrate di Ricerca. In L'Anatolie des Peuples, des Cités et des Cultures (IIe millénaire av. J.-C.—Ve siècle ap. J.-C.).Colloque International de Besançon. 26–27 Novembre 2010. Volume 2. Approches Locales et Régionales. 2013. Available online: https://www.persee.fr/doc/ista_0000-0000_2013_act_1277_2_3752 (accessed on 20 August 2024).
41. Ozan, A.; Dedeoglu, F.; Konakci, E. Prehistory of the Lykos Valley. In *Landscape and History in the Lykos Valley: Laodikeia and Hierapolis in Phrygia*; Şimşek, C., D'Andria, F., Eds.; Cambridge Scholars Publishing: Cambridge, UK, 2016; pp. 47–71.
42. Scardozzi, G. Marmora Phrygiae Project: The Contribution of Landscape Archaeology Research in the Territory of Hierapolis in Phrygia to the Reconstruction of Building Sites in the City and Their Strategies for Supplying Stone Materials. In *Landscape and History in the Lykos Valley: Laodikeia and Hierapolis in Phrygia*; Şimşek, C., D'Andria, F., Eds.; Cambridge Scholars Publishing: Cambridge, UK, 2016.
43. Özler, H.M. Water Balance and Water Quality in the Çürüksu Basin, Western Turkey. *Hydrogeol. J.* **1999**, *7*, 405–418. [CrossRef]
44. Gülmez, F.; Damci, E.; Ülgen, U.B.; Okay, A. Deep Structure of Central Menderes Massif: Data from Deep Geothermal Wells. *Turk. J. Earth Sci.* **2019**, *28*, 531–543. [CrossRef]
45. Alçiçek, H.; Varol, B.; Özkul, M. Sedimentary Facies, Depositional Environments and Palaeogeographic Evolution of the Neogene Denizli Basin, SW Anatolia, Turkey. *Sediment. Geol.* **2007**, *202*, 596–637. [CrossRef]
46. Hughes, J.J.; van Balen, K.; Bicer-Simsir, B.; Binda, L.; Elsen, J.; van Hees, R.; Von Konow, T.; Lindqvist, J.E.; Maurenbrecher, P. RILEM TC 203-RHM: Repair Mortars for Historic Masonry: The Role of Mortar in Masonry: An introduction to requirements for the design of repair mortars. *Mater. Struct.* **2012**, *45*, 1287–1294. [CrossRef]
47. Pecchioni, E.; Fratini, F.; Cantisani, E. *Atlas of Ancient Mortars in Thin Section under Optical Microscope*, 2nd ed.; Nardini: Firenze, Italy, 2020; p. 78.
48. Pouchou, J.L.; Pichoir, F. Quantitative Analysis of Homogeneous or Stratified Microvolumes Applying the Model "PAP". In *Electron Probe Quantitation*; Springer: Boston, MA, USA, 1991; pp. 31–75.
49. Seymour, L.M.; Keenan-Jones, D.; Zanzi, G.L.; Weaver, J.C.; Masic, A. Reactive Ceramic Aggregates in Mortars from Ancient Water Infrastructure Serving Rome and Pompeii. *Cell Rep. Phys. Sci.* **2022**, *3*, 101024. [CrossRef]
50. Whitney, D.L.; Evans, B.W. Abbreviations for Names of Rock-Forming Minerals. *Am. Mineral.* **2010**, *95*, 185–187. [CrossRef]
51. Warr, L.N. IMA-CNMNC Approved Mineral Symbols. *Mineral. Mag.* **2021**, *85*, 291–320. [CrossRef]
52. McConnell, J.D.C. Vaterite from Ballycraigy, Lame, Northern Ireland. *Mineral. Mag.* **1960**, *32*, 748–749.
53. Christy, A.G. A Review of the Structures of Vaterite: The Impossible, the Possible, and the Likely. *Cryst. Growth Des.* **2017**, *17*, 3567–3578. [CrossRef]
54. Ruiz-Agudo, E.; Putnis, C.V.; Hövelmann, J.; Álvarez-Lloret, P.; Ibáñez-Velasco, A.; Putnis, A. Experimental Study of the Replacement of Calcite by Calcium Sulphates. *Geochim. Et Cosmochim. Acta* **2015**, *156*, 75–93. [CrossRef]

55. Vettori, S.; Cabassi, J.; Cantisani, E.; Riminesi, C. Environmental Impact Assessment on the Stone Decay in the Archaeological Site of Hierapolis (Denizli, Turkey). *Sci. Total Environ.* **2019**, *650*, 2962–2973. [CrossRef]
56. Rampazzi, L. Calcium Oxalate Films on Works of Art: A Review. *J. Cult. Herit.* **2019**, *40*, 195–214. [CrossRef]
57. Cosano, D.; Esquivel, D.; Jiménez-Sanchidrián, C.; Ruiz, J.R. Analysis of Mortars from the Castle Keep in Priego de Cordoba (Spain). *Vib. Spectrosc.* **2021**, *112*, 103184. [CrossRef]
58. Frankeová, D.; Koudelková, V. Influence of Ageing Conditions on the Mineralogical Micro-Character of Natural Hydraulic Lime Mortars. *Constr. Build. Mater.* **2020**, *264*, 120205. [CrossRef]
59. Peters, T.; Iberg, R. Mineralogical Changes During Firing of Calcium-Rich Brick Clays. *Ceram. Bull.* **1978**, *57*, 503–509.
60. Dondi, M.; Ercolani, G.; Fabbri, B.; Marsigli, M. An Approach to the Chemistry of Pyroxenes Formed during the Firing of Ca-Rich Silicate Ceramics. *Clay Miner.* **1998**, *33*, 443–452. [CrossRef]
61. Boynton, R.S. *Chemistry and Technology of Lime and Limestone*, 2nd ed.; John Wiley & Sons: New York, NY, USA, 1980.
62. Hancock, P.L.; Chalmers, R.M.L.; Altunel, E.; Çakir, Z.; Becher-Hancock, A. *Creation and Destruction of Travertine Monumental Stone by Earthquake Faulting at Hierapolis, Turkey*; Geological Society: London, UK, 2000; pp. 1–14. [CrossRef]
63. Di Giacomo, G. The On-Line Platform of the Marmora Phrygiae Project. Ancient Quarries and Building Sites in Asia Minor. In *Research on Hierapolis in Phrygia and Other Cities in South-Western Anatolia: Archaeology, Archaeometry, Conservation*; Edipuglia: Bari, Italy, 2016; pp. 33–41.
64. Arthur, P. *Hierapolis of Phrygia: The Drawn-Out Demise of an Anatolian City*; Routledge: London, UK, 2012.
65. Ismaelli, T.; Scardozzi, G.; Bozza, S.; Ungaro, R. The Early Byzantine City Walls of Hierapolis in Phrygia: Demolishing and Recycling the Imperial Era Monuments. *Acta Ad Archaeol. Et Artium Hist. Pertin.* **2021**, *33*, 19. [CrossRef]
66. El Ouahabi, M.; Daoudi, L.; Hatert, F.; Fagel, N. Modified Mineral Phases During Clay Ceramic Firing. *Clays Clay Miner.* **2015**, *63*, 404–413. [CrossRef]
67. Stefanidou, M.; Papachristoforou, M.; Kesikidou, F. Fiber-Reinforced Lime Mortars. In Proceedings of the 4th Historic Mortars Conference, Santorini, Greece, 10–12 October 2016.
68. Calandra, S.; Barone, S.; Cantisani, E.; Caggia, M.P.; Liccioli, L.; Vettori, S.; Fedi, M. Radiocarbon Dating of Straw Fragments in the Plasters of St. Philip Church in Archaeological Site Hierapolis of Phrygia (Denizli, Turkey). *Radiocarbon* **2023**, *65*, 323–334. [CrossRef]